VPS VIBRATIONS IN PHYSICAL SYSTEMS

DOI: 10.21008/j.0860-6897.2024.1.08
Vibrations in Physical Systems, 2024, 35(1), 2024108

Acoustic metamaterial design for levelling the impact of double-wall resonance on sound insulation

Aleksandra KLIMEK, Andrzej DOBRUCKI

[1] Department of Acoustics, Multimedia and Signal Processing, Wroclaw University of Science and Technology, 27 Wybrzeże Wyspiańskiego St., 50-370 Wroclaw, Poland,

Corresponding author: Aleksandra KLIMEK, email: aleksandra.klimek@pwr.edu.pl

Abstract This paper presents two solutions employing locally resonant metamaterial to level the mass-air-mass resonance impact on the sound insulation. The first operates on the cantilever beam resonance, and the second uses masses vibrating in flexural mode cut out from the additional panel. Both structures are mounted between two lightweight, honeycomb cardboard panels with a double-wall resonance of 420 Hz. Solutions were analysed numerically for their vibration and acoustic properties and measured in the reverberation chamber, resulting in information about the dispersion curve, effective dynamic mass, and sound insulation. The analytical results of Sound Transmission Loss (STL) and the experimental measurements of diffused-field Sound Reduction Index (SRI) proved the existence of sound-insulation enhancement. The local rise in SRI resulted in an increase of broadband Weighted SRI up to 5 dB.

Keywords: plate-type, acoustic metamaterial, sound insulation, transmission loss, FEA, cardboard.

1. Introduction

The application of Acoustic Metamaterials (AMMs) holds immense potential for enhancing the sound insulation performance of partitions. These artificially engineered materials offer unique properties allowing precise control over sound wave propagation. Conventional sound insulation methods rely on mass and damping properties to reduce sound transmission. However, acoustic metamaterials introduce a novel approach by exploiting the concept of negative density or negative bulk modulus, enabling the control of wave propagation at subwavelength scales for specific frequency ranges. This unique characteristic allows for the design of compact and lightweight materials. Various metamaterials types have been employed to achieve improved sound transmission control, including negative bulk modulus metamaterials with periodically arranged Helmholtz resonators [1], and negative density metamaterials with local resonances, such as plate-type metamaterials with periodically arranged masses attached to a plate [2–5] or membrane-type metamaterials with masses embedded in the elastic layer [6, 7].

The particular metamaterial application is tuning its frequency range to match the drop in existing transmission loss, for example, the mass-air-mass resonance of the double wall. The reduced mass of lightweight partitions leads to a higher mass-air-mass resonance frequency, resulting in lower sound insulation performance compared to heavier constructions. To address this issue, the metamaterial inclusions could be incorporated into the double-wall system enhancing the transmission loss within the given resonance frequency range and consequently counteract it with simultaneous maintenance of the whole structure's low weight [1, 2].

In this article, we present two plate-type AMM designs specifically tailored to affect the resonant behaviour of double walls. These designs employ paper-based products: paperboard metamaterial resonators placed between the two honeycomb cardboard partition walls, which results in a sustainable and lightweight structure (Fig. 1). In order to evaluate the effectiveness of the suggested designs, we conduct numerical simulations using the ANSYS 2022 R1 Finite Element Analysis (FEA) software. The sound transmission loss and dispersion relation are analysed, providing the effectiveness of the metamaterial inclusions. Furthermore, experimental measurements of the Sound Reduction Index (SRI) are performed using the intensity probe method in a reverberation chamber, validating the sound insulation capabilities of the proposed designs.

a)

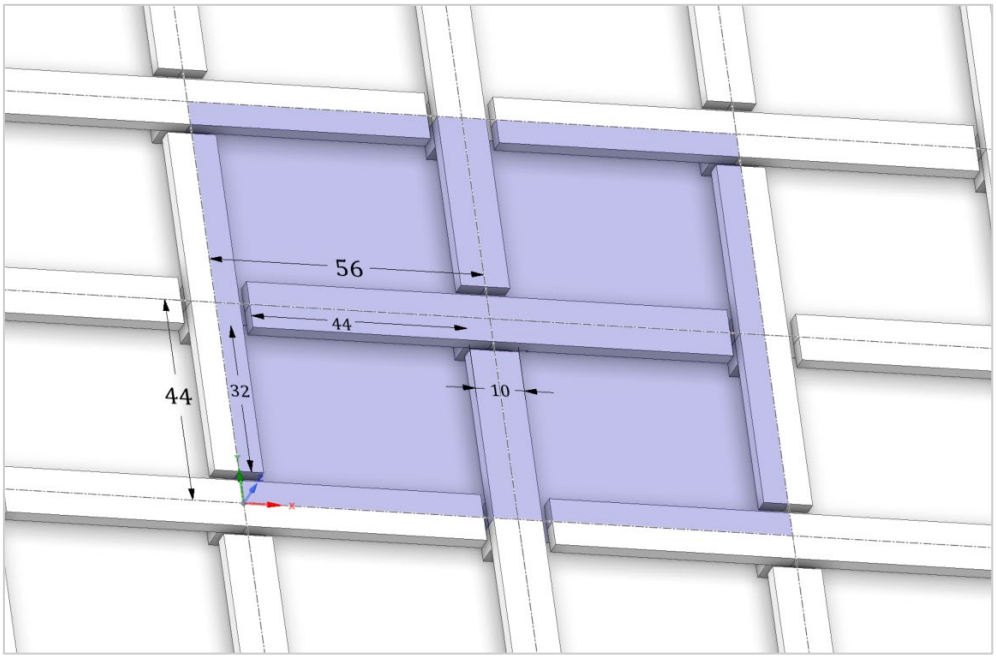

b)

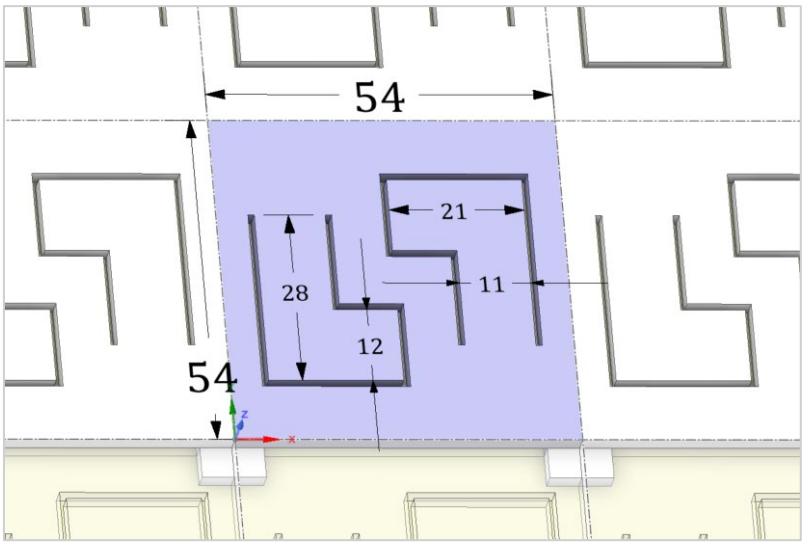

Figure 1. The schemes of proposed metamaterial designs:
a) type A with cantilever beams, b) type B with masses cut in additional panel.
Structures are mounted on one of the base walls. Every dimension is given in millimetres.
The unit cell is marked with colour blue.

The structure of this article is as follows. Section 2 presents the theoretical framework underlying the sound insulation of double walls with the addition of metamaterials. Section 3 outlines the materials and methods employed, including the numerical simulations and experimental procedures. Section 4 gives the achieved results and discusses their implications. Section 5 provides a conclusive summary of the findings and future research directions.

2. Theory

The sound insulation performance of double walls relies on the occurrence of mass-spring-mass resonance, which arises from the interaction between the mass of the partition walls and the compressibility of the air within the enclosed air cavity. The resonance frequency, denoted as f_0, can be determined using the equation [8, 9]:

$$f_0 = \frac{1}{2\pi}\sqrt{\frac{\rho_0 c_0^2 (m'_a + m'_b)}{m'_a m'_b d}}. \tag{1}$$

In this equation, ρ_0 represents the air density, c_0 is the speed of sound in air, m'_a and m'_b correspond to the surface masses of the two partition walls: a, b, and d is the distance between the walls. It is important to note that in lightweight double walls, the reduced mass of the partitions results in a higher resonance frequency. This higher frequency range is often associated with reduced sound insulation capabilities since the transmission loss decline is shifted towards the audible band.

The Sound Transmission Loss (STL) of a double wall, according to the *Multiple refraction theory,* is as follows [2, 8]:

$$STL(\theta) = -10\log_{10}\big(\tau(\theta)\big) = -10\log_{10}\left|\frac{\sqrt{\tau_a}\sqrt{\tau_b}}{1-\alpha\big(1-\sqrt{\tau_a}\big)\big(1-\sqrt{\tau_b}\big)e^{-2jkd\cos\theta}}\right|^2, \tag{2}$$

where θ is the incident wave angle, α is the reflection coefficient, k is the wavenumber of air, and the $\tau_{a,b}$ are the transmission coefficients of panels a and b respectively:

$$\frac{1}{\tau_{a,b}} = \left|1 + \frac{j\omega m'_{a,b}\cos\theta}{2\rho_0 c_0}\right|^2, \tag{3}$$

where ω stands for the angular frequency; $\omega = 2\pi f$. The diffused-field transmission coefficient $\bar{\tau}$ is then integrated over every wave incident angle, in this case from 0 to maximum angle θ_l:

$$\bar{\tau} = \frac{\int_0^{\theta_l} \tau\cos\theta\sin\theta\, d\theta}{\int_0^{\theta_l}\cos\theta\sin\theta\, d\theta}, \tag{4}$$

A single cell of metamaterial addition could be represented mechanically as a resonator with mass m_2 and a damping ratio ζ_2, which is connected to a plate with a mass m_1 through spring with stiffness k_2 (Fig. 2).

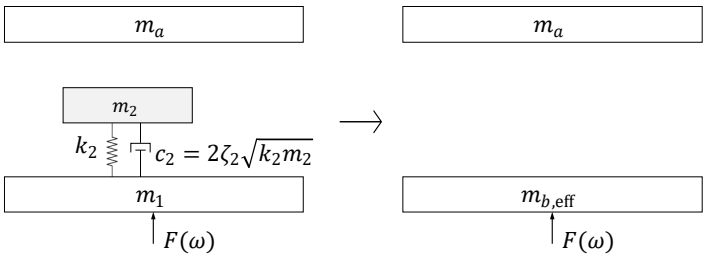

Figure 2. Schematic diagrams of single cell mass spring resonator. The diagram on the left represents the actual mass distribution and the diagram on the right portray the dynamic effective mass.

The resonance frequency of such connection equals $\omega_2 = \sqrt{k_2/m_2}$. By analysing the equations of motion of this system in response to excitation by force $F(\omega)$ applied to mass m_1, it is possible to reduce it to an equivalent system with a single dynamic mass, denoted as m_{eff} [2]:

$$m_{b,\mathrm{eff}} = m_1 + m_2\left[\frac{\frac{2j\zeta_2\omega}{\omega_2}+1}{1+\frac{2j\zeta_2\omega}{\omega_2}-\frac{\omega^2}{\omega_2^2}}\right]. \tag{5}$$

When the frequency ω is slightly above the resonance frequency ω_2, there is a range where the effective dynamic mass can become negative. This causes the structure to become a negative-density acoustic metamaterial. By incorporating the resulting equivalent mass, equation (3) can be modified to calculate the transmission loss of a metamaterial plate.

Equation (5) requires parameters that are often difficult to predict accurately in real-world applications. The approach proposed by de Melo Filho et al. [2] focuses on incorporating the stop-band effect of metamaterials. The key aspect is calculating the dynamic mass of the metamaterial panel by relating the

stop band limits obtained from dispersion curves to the negative mass frequency region. Equation (5) has been modified to necessitate solely the knowledge of the combined mass of m_1 and m_2:

$$m_{b,\text{eff}} = (m_1 + m_2) + \frac{(m_1 + m_2)}{1 - \dfrac{1}{1 - \dfrac{\omega_H^2}{\omega_L^2}}} \left[\frac{\dfrac{2j\zeta_2\omega}{\omega_L} + 1}{1 + \dfrac{2j\zeta_2\omega}{\omega_L} - \dfrac{\omega^2}{\omega_L^2}} - 1 \right]. \tag{6}$$

The damping ratio ζ_2 is obtainable through direct measurement. ω_L represents the actual resonance frequency that emerges within the structure. Beyond this frequency, the effective mass $m_{b,\text{eff}}$ becomes negative and continues in negativity up to the frequency ω_H. The negative mass region coincides with the band gap region, allowing the acquisition of the angular frequencies ω_L and ω_H from the dispersion relation.

2.1. Dispersion curves of acoustic metamaterial

The dispersion curves reveal the relationship between wave frequency and wave vector, showcasing how the material alters the propagation properties of different wave modes. From the dispersion curves, one can gather information such as the presence and location of bandgaps, which indicate the frequency ranges where specific wave modes are prohibited or strongly suppressed within the metamaterial. The band gaps coincide with the frequency region of negative mass. The dispersion relation can be derived from the solution of the Bloch-Floquet theorem [10–12]:

$$\mathbf{u}(x) = \mathbf{u}(x_0)e^{i\mathbf{k}(x-x_0)}. \tag{7}$$

Here, $\mathbf{u}(x)$ and $\mathbf{u}(x_0)$ represent the displacement vectors at respective locations x and x_0, and $\mathbf{k}$ denotes the wave vector (Floquet wavenumber) over the Brillouin contour. This relation leads to an eigenvalue problem with predefined values of $\mathbf{k}$, and the results can be obtained using FEA through modal analysis. The locations x and x_0 are the boundaries of the indivisible unit cell. In a model with a lattice structure repeatable in two directions, the Brillouin Zone with all possible $\mathbf{k}$ vectors are depicted in Figure 3a, using the example of type B metamaterial geometry. Consequently, for each $\mathbf{k}$ value in the x and y directions, ranging from point Γ through X, M, and back to Γ, an individual modal analysis is conducted. The resulting band structures for both metamaterial designs are depicted in Fig. 3b and 3c. The lower and upper limit of the band gap (marked with the colour grey) stands for the angular frequencies ω_L and ω_H.

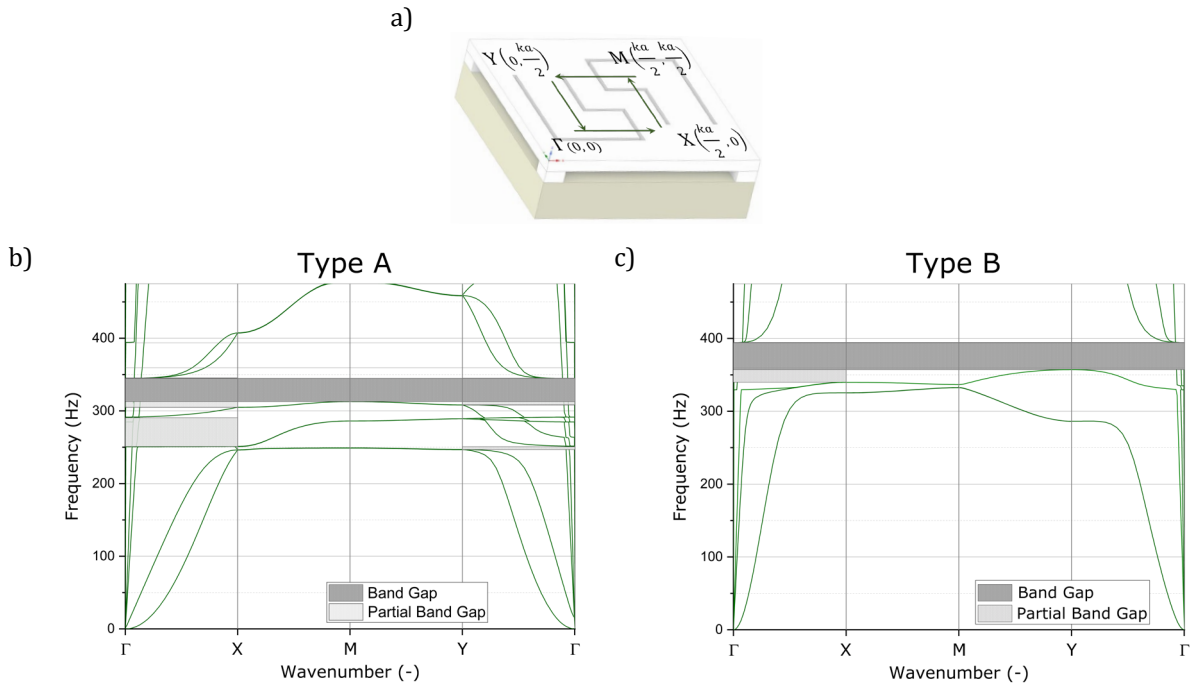

Figure 3. a) First Brillouin zone scheme on the example of metamaterial type B, and dispersion curves of metamaterials: b) type A, c) type B.

3. Materials and methods

The subsequent section presents a comprehensive depiction of the structures, containing their dimensions and mechanical properties. It also includes a detailed explanation of the numerical models employed and provides information on the conducted measurements of the sound reduction index.

3.1. Materials

The structure labelled as A in the metamaterial configuration comprises cantilever beams that are firmly attached at their midpoint to a base flat panel using holders. The metamaterial structure B includes an additional panel with resonators that have been cut into it, also mounted by holders to the base flat panel. In both cases, the entire plate exhibits periodicity in the XY plane and is excited by an incident plane wave propagating along the Z axis. Figure 1 highlights the individual unit cell, distinguished by a blue colour. The base panels are d=60 mm apart and have a thickness of 10 mm, while all other resonant components (such as beams, additional panel, and holders) have a thickness of 3 mm. Fig. 4 showcases photographs of the metamaterial structures.

a) b)

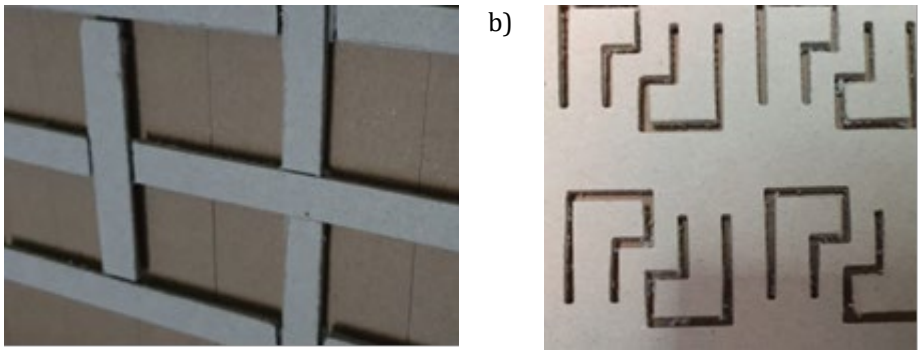

Figure 4. Photographs of metamaterial structures a) type A, b) type B.

The materials employed in the simulations are orthotropic, where cardboard is used for the additional structures, and paper honeycomb is used for the base panel. Notably, due to the cardboard's orthogonal nature, the measurements were conducted in both the machine direction (MD) and cross-machine direction (CD). The beams in metamaterial A are intentionally designed with different lengths to achieve a matching resonance frequency between the beams, and therefore, to simplify the mechanic representation to that of single degree of freedom, as presented on the Fig. 2. This is accomplished by considering the varying Young's modulus in the X and Y directions, ensuring that the projected resonance frequencies align closely. Table 1 provides a comprehensive overview of all the material parameters.

Table 1. Mechanical parameters of metamaterials components type A and B.

Element	Quantity	Symbol	Direction	Value
Beams, additional panel, and holders	Young Modulus	E	y (CD) & z	1.0 GPa
			x (MD)	2.0 GPa
	Damping ratio	ζ_2	every	0.069
	Volumetric density	ρ	-	667 kg/m^3
Base panel	Young Modulus	E	Every	0.11 GPa
	Density	ρ	-	76 g/m^3

3.2. Methods

The numerical analysis was performed using ANSYS 2022 R1 software, employing the following: Modal Analysis to obtain the dispersion relation and Harmonic Acoustics to calculate the Transmission Loss. Both simulations were carried out on a single unit cell, considering periodic boundary conditions [10, 11, 13].

This paper utilizes two measurement methods: the vibration-damping properties of metamaterials components, and laboratory measurements of AMMs sound insulation.

The vibration-damping properties were measured using the beam resonance method (based on the ASTM E-756 standard [14]) for dynamic Young's modulus E and damping ratio ζ_2. The method involved non-contact measurement of the frequency and quality factor of cantilever beam resonance. A Polytec PSV-

400 laser vibrometer was used to capture the beam's vibration velocity, while a Brüel & Kjær MM002 magnetic transducer with a chirp signal excited the beam.

Laboratory measurements of sound insulation were performed in a reverberation chamber (based on the ISO standard 15186-1 [15] for the weighted modified intensity Sound Reduction Index ($R_{I,M,W}$) in 1/3 octave bands. The measurements involved clamping a sample with dimensions of 1162 mm x 865 mm in the opening of a reverberation transmitting chamber with non-parallel walls and a volume of 67 m^3. The joint between the clamping frame and the sample was sealed with butyl and a layer of EPDM rubber. A Norsonic 276 reference sound source was used to create a diffuse sound field within the chamber, and the resulting average sound pressure level was measured at locations representative of the sound energy impacting the sample. The sound intensity probe, with Gras 40GK 1/2" microphones located 100 mm from the sample surface and a 50 mm probe microphone separator, captured the signal outside the chamber using a sweeping method.

4. Results

The results section presents the analytical evaluation of Sound Transmission Loss (STL) under two conditions: plane wave excitation and diffused field excitation. Additionally, the analytical results are specifically compared to the measured Sound Reduction Index (SRI) results obtained under the diffused field. This comparison provides valuable insights into the agreement between the analytical predictions and the experimental measurements.

4.1. Analytical results

Figure 5 presents the analytical results of STL for two types of metamaterials, A and B, obtained with the equations (2)-(4), and (6). The upper row illustrates the results for plane wave excitation, while the bottom row showcases the STL in the diffused field. The STL of the metamaterials is compared to that of a double wall, specifically a simple double wall consisting of two honeycomb plates, and an equivalent mass double wall where one plate's mass is increased by the mass of resonant elements.

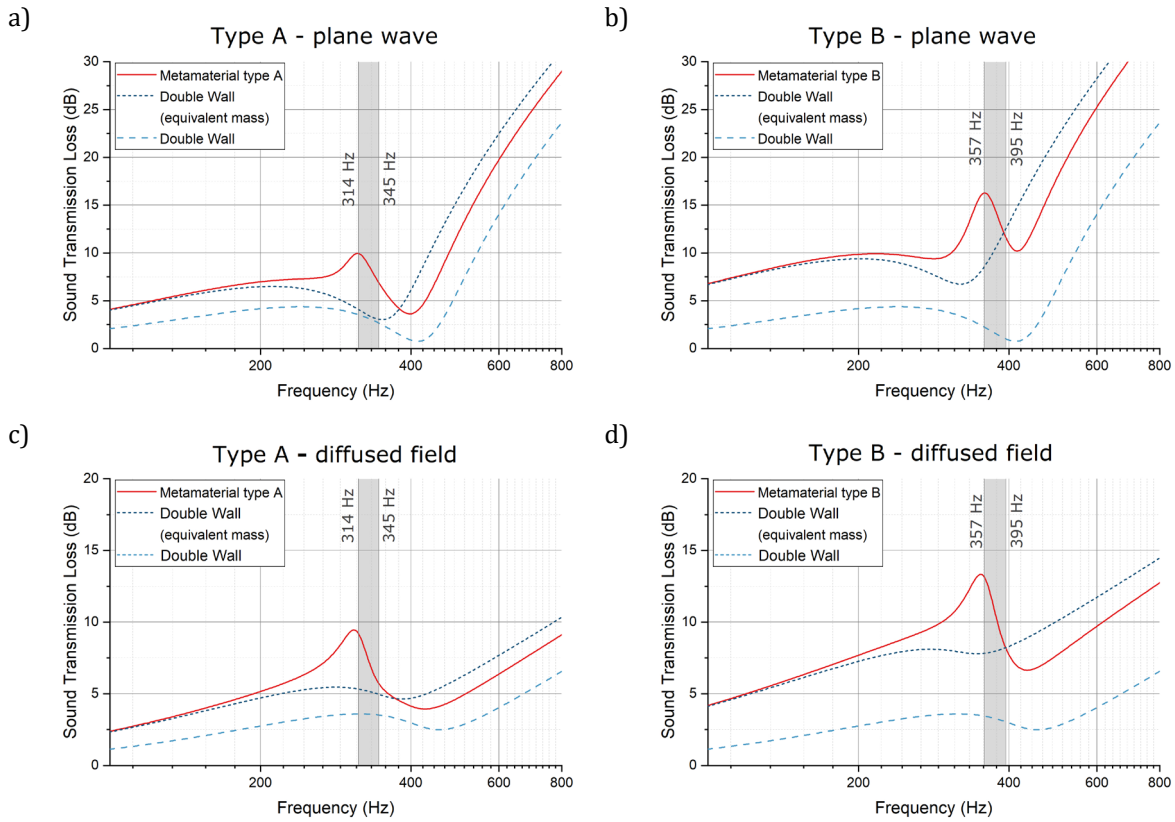

Figure 5. Analytical results of Sound Transmission Loss of metamaterials (red line) compared to the double wall with equivalent mass (dark blue dotted line) and double wall without additional mass (light blue dashed line). Band gaps are represented by grey area. Excitation by the plane wave: a) type A, and b) type B; and under diffused field: c) type A, d) type B.

Both metamaterial types demonstrate a substantial increase in STL within the frequency range of their respective band gaps. This improvement addresses the limited effectiveness of the double wall's sound transmission loss near its mass-air-mass resonance. Metamaterial Type A achieves an increase of 5.9 dB, while metamaterial Type B achieves an increase of 9.8 dB. However, for frequencies slightly above the upper limit of the band gap, the metamaterials exhibit a drop in STL. Consequently, the overall STL above this threshold is lower compared to a structure with equivalent mass. This dependence is not observed when comparing the metamaterials to the host structure alone.

The presence of a diffused field does not impact the frequency of the STL peak for the metamaterials. However, it does affect the frequency of the lowest point in the STL value for the double wall configuration. As a result, the difference between these two frequencies changes under different excitations. In the case of metamaterial Type A, where the STL peak frequency is slightly lower than the resonance of an equivalent mass double wall, the introduction of a diffused field does not contribute to the improvement of STL within this range. Conversely, for metamaterial Type B, the frequency of the STL peak aligns closely with the drop in STL observed in the diffused field for the equivalent mass double wall, and consequently, the STL near double-wall resonance improves.

Overall, the addition of metamaterials significantly enhances the double wall insulation properties.

4.2. Measurements results

The measurement results of sound transmission are presented in Figure 6, where the Sound Reduction Index (SRI) of the Acoustic Metamaterials (AMMs) is compared to the SRI of a double wall without any additional masses. In the bottom row of Figure 6, the measured SRI increase is compared to the analytical results.

The comparison reveals, that in the case of metamaterial Type B, the peak SRI increase aligns well with the theoretical peak frequency. There is a good agreement between the measured and analytical results for metamaterial Type B. Any discrepancy below 200 Hz could be originated by resonances arising within the reverberation room. However, in the case of metamaterial Type A, the agreement between the measured and analytical results is not as strong.

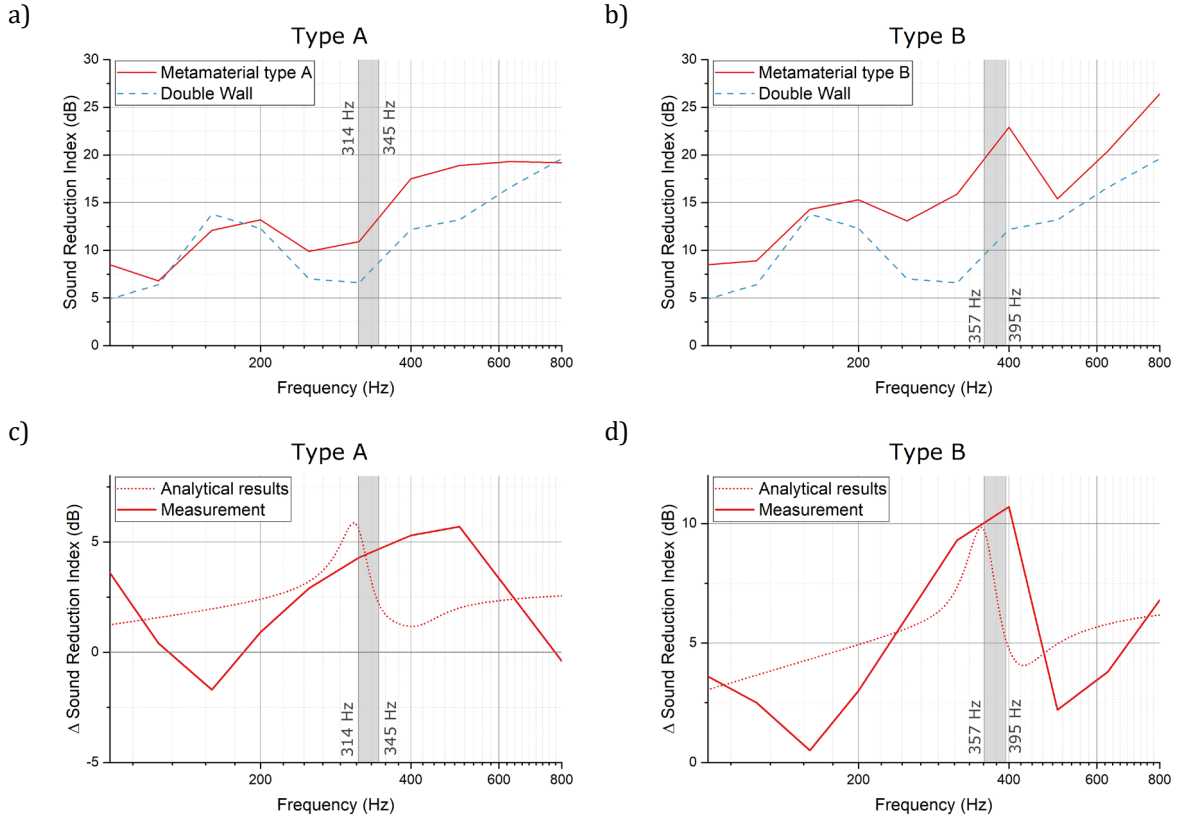

Figure 6. Measurements results of Sound Reduction Index metamaterials (red line) compared to the double wall (light blue dashed line). Band gaps are represented by grey area: a) type A, and b) type B. Measurement results of metamaterials' SRI (solid line) compared to the analytical results (dotted line) c) type A, and d) type B.

Several factors may have contributed to these differences. One factor is the limitation of the 1/3 octave band measurement technique used, which does not capture the complete frequency response accurately. Additionally, the mechanical properties of paper, such as the inconsistent Young's modulus throughout the structure volume, due to the paper production process, could have influenced the width of the resonance.

Comparing the two metamaterial types, Type B demonstrates better performance. This can be attributed not only to the higher surface mass of the metamaterial additions but also to the higher repeatability of the structure. The repeatability is achieved by cutting the springs of the local resonators in the metamaterial only in the Y direction, allowing for a consistent local resonance frequency throughout the metamaterial structure. On the other hand, in the case of metamaterial Type A, the structure is more sensitive to technical difficulties during the manufacturing process. One possible reason could be the inadequate stiffness of a holder, stemming from the potential delamination, leading to the emergence of a bending mode within the holder body rather than the desired bending mode within the beam. This would result in the resonator applying a reduced force to the plate in the z-direction, consequently diminishing its effectiveness.

The weighted Sound Reduction Index (SRI) of the host double-wall structure is 19 dB, while for metamaterial Type A, it is 22 dB, and for metamaterial Type B, it is 24 dB. This indicates an increase in the whole frequency band of 3 dB and 5 dB, respectively, highlighting the effectiveness of the metamaterials in enhancing sound reduction.

5. Conclusions

This study presented two plate-type Acoustic Metamaterial (AMM) designs aimed at addressing the mass-air-mass resonance impact on sound insulation. The designs incorporated locally resonant elements, including cantilever beams (type A) and masses cut into an additional panel (type B), placed between lightweight honeycomb cardboard partition walls. Numerical simulations and experimental measurements were conducted to evaluate the effectiveness of the proposed designs.

Analytical results of Sound Transmission Loss (STL) and experimental measurements of the diffused-field Sound Reduction Index (SRI) demonstrated the enhancement of sound insulation provided by the metamaterials. Both metamaterial types showed a significant increase in STL within the frequency range of their respective band gaps. The peak STL increase, within the band gap presence, equals 5.9 dB in case of metamaterial type A, and 9.8 dB in case of metamaterial type B.

The measured SRI results compared to the analytical results showed good agreement for metamaterial Type B, where the peak SRI increase coincided well with the theoretical peak frequency. However, the agreement between the measured and analytical results was not as strong for metamaterial type A. Possible factors contributing to these differences include maintaining a consistent local resonance frequency throughout the metamaterial structure. In contrast, the structure of metamaterial Type A was more sensitive to manufacturing difficulties. This factor also affected the metamaterial type B better performance compared to type A.

The introduction of the metamaterials resulted in an increase in the weighted SRI, with the host double-wall structure having an SRI of 19 dB, metamaterial type A achieving 22 dB, and metamaterial type B reaching 24 dB. This corresponded to an increase in the whole frequency band of 3 dB and 5 dB, respectively, demonstrating the effectiveness of the metamaterials in improving sound insulation. In conclusion, the application of locally resonant metamaterials showed promising results in enhancing the sound insulation properties of double walls. Further research and development in this field could lead to the design and implementation of more efficient solutions.

Acknowledgments

This research was supported by the National Centre for Research and Development of Poland, grant number Lider/60/0250/L-11/ 19/NCBR/2020.
The authors thank the KFB Acoustics for providing with the laboratory equipment, necessary to conduct reliable tests.

Additional information

The authors declare: no competing financial interests and that all material taken from other sources (including their own published works) is clearly cited and that appropriate permits are obtained.

References

1. F. Langfeldt, H. Hoppen, W. Gleine; Broadband low-frequency sound transmission loss improvement of double walls with Helmholtz resonators; J Sound Vib, 2020, 476, 1–16; DOI: 10.1016/j.jsv.2020.115309
2. N.G.R. de Melo Filho, L. Van Belle, C. Claeys, E. Deckers, W. Desmet; Dynamic mass based sound transmission loss prediction of vibro-acoustic metamaterial double panels applied to the mass-air-mass resonance; J Sound Vib, 2019, 442, 28–44; DOI: 10.1016/j.jsv.2018.10.047
3. Y. Xiao, J. Wen, X. Wen; Sound transmission loss of metamaterial-based thin plates with multiple subwavelength arrays of attached resonators; J Sound Vib, 2012, 331(25), 5408–5423; DOI: 10.1016/j.jsv.2012.07.016
4. J.H. Vazquez Torre, J. Brunskog, V. Cutanda Henriquez; An analytical model for broadband sound transmission loss of a Finite Single Leaf Wall using a two degree of freedom resonant Metamaterial; Proc Int Congr Acoust, 2019, 2019-Septe(1), 2091–2098; DOI: 10.18154/RWTH-CONV-239598
5. L. Van Belle, C. Claeys, E. Deckers, W. Desmet; The impact of damping on the sound transmission loss of locally resonant metamaterial plates; J Sound Vib, 2019, 461, 114909; DOI: 10.1016/j.jsv.2019.114909
6. C.J. Naify, C.M. Chang, G. McKnight, S. Nutt; Transmission loss and dynamic response of membrane-type locally resonant acoustic metamaterials; J Appl Phys, 2010, 108(11); DOI: 10.1063/1.3514082
7. C.J. Naify, C.M. Chang, G. McKnight, F. Scheulen, S. Nutt; Membrane-type metamaterials: Transmission loss of multi-celled arrays; J Appl Phys, 2011, 109(10); DOI: 10.1063/1.3583656
8. K.A. Mulholland, H.D. Parbrook, A. Cummings; The transmission loss of double panels; J Sound Vib, 1967, 6(3), 324–334; DOI: 10.1016/0022-460X(67)90205-2
9. J. Wang, T.J. Lu, J. Woodhouse, R.S. Langley, J. Evans; Sound transmission through lightweight double-leaf partitions: Theoretical modelling; J Sound Vib, 2005, 286(4–5), 817–847; DOI: 10.1016/j.jsv.2004.10.020
10. C. Hakoda, J. Rose, P. Shokouhi, C. Lissenden; Using Floquet periodicity to easily calculate dispersion curves and wave structures of homogeneous waveguides; In: AIP Conference Proceedings. American Institute of Physics Inc. 2018
11. A. Melnikov, M. Hankec, S. Marburg; Dispersion Curves of Elastic Metamaterials and Sonic Crystals with ANSYS Pianissimo-Development of Noise Optimized Stage Elevator View project; In: 36. CADFEM ANSYS Simulation Conference, 2018
12. A. Klimek; Fluid-Fluid Phononic Crystal with Elastic Coat Working in Audible Frequencies; Vib. Phys. Syst., 2019, 30(1), 2019145
13. A.D. Canonsburg; Acoustic Analysis Guide; January 2019
14. ASTM E-756; Standard Test Method for Measuring Vibration-Damping Properties of Materials; Annu B ASTM Stand, 2005, 05(Reapproved 2017), 14; DOI: 10.1520/E0756-05R17.2
15. ISO 15186-1:2000; Acoustics — Measurement of sound insulation in buildings and of building elements using sound intensity — Part 1: Laboratory measurements; ISO, 2000